2-14-2020

Optimal power routing scheme between and within interlinking converters in unbalanced hybrid AC–DC microgrids

Mohammad Mahmoudian Esfahani
Florida International University

Hany F. Habib
Florida International University

Osama A. Mohammed
Florida International University

IET Generation, Transmission & Distribution

Research Article

IET Journals
The Institution of Engineering and Technology

Optimal power routing scheme between and within interlinking converters in unbalanced hybrid AC–DC microgrids

ISSN 1751-8687
Received on 10th January 2019
Revised 6th September 2019
Accepted on 16th October 2019
E-First on 19th December 2019
doi: 10.1049/iet-gtd.2019.0061
www.ietdl.org

Mohammad Mahmoudian Esfahani[1], *Hany F. Habib*[1], *Osama A. Mohammed*[1] ✉

[1]*Department of Electrical and Computer Engineering, Florida International University, Miami, FL 33174, USA*

✉ *E-mail: mohammed@fiu.edu*

Abstract: An optimal power routing (OPR) scheme between and within interlinking converters (ICs) in unbalanced hybrid AC–DC microgrids to minimise the power imbalance factor at the point of common coupling, active power losses, and voltage deviation indices for microgrids in grid-connected operating mode is proposed in this study. These goals are achieved through a multi-objective optimisation model by optimal distributing of mobile loads between available charging stations and at the same time, OPR within three phases of three-phase four-lag AC/DC converters. Numerical results obtained from implementing the proposed method on the modified IEEE 13-bus system, as an unbalanced hybrid microgrid, and IEEE 34-bus test system, as an unbalanced distribution system, demonstrate that proposed OPR algorithm is successful to satisfy the optimisation goals. For this purpose, four case studies are defined and studied to demonstrate the unique features of the proposed OPR comparing with other power routing schemes. In addition to simulation results, the OPR scheme between ICs is realistically implemented at Florida International University smart grid testbed to show the effect of the power routing on energy losses reduction.

Nomenclature

$\boldsymbol{A}$	coefficient matrix
APLI_c	active power losses index for cth case study
$\text{APLI}^{\max}$	maximum APLI among all case studies
$\tilde{A}_c$	normalised APLI_C
$\text{Ave}\lvert V_i^k \rvert$	average voltage magnitude of three phases at ith bus
$\boldsymbol{B}$	vector of upper bands
D	number of the buses connected to ICs
$f_i(X)$	ith objective function
I_j^k	current of kth phase of jth line
$I_j^{\max}$	maximum current for each phase of jth line
k, m	phase indicators in a three-phase system (a,b,c)
L	number of transmission lines
MOI_c	microgrid operating index for cth case study
$\text{MOI}^{\max}$	maximum MOI among all case studies
$\tilde{M}_c$	normalised MOI_C
N	number of buses in the system
PIFI_c	power imbalance factor index for cth case study
$\text{PIFI}^{\max}$	maximum PIFI among all case studies
$\tilde{P}_c$	normalised PIFI_C
$P_d^k,\ Q_d^k$	active and reactive power set point for kth phase of dth ICs
$P_d^{\text{ref},k},\ Q_d^{\text{ref},k}$	reference active and reactive power for kth phase of dth ICs.
$P_d^{\text{Opt},k},\ Q_d^{\text{Opt},k}$	optimum active and reactive power set points for kth phase of dth ICs.
$P_d^{\min}, P_d^{\max}$	minimum/maximum active power limit for each phase of dth ICs
PT_d	total active power of dth ICs
$PT_d^{\min}, PT_d^{\max}$	minimum/maximum total active power limit for dth ICs
$P_i^k + \text{j}Q_i^k$	injected complex power from the kth phase of the ith bus to the grid
$Q_d^{\min}, Q_d^{\max}$	minimum/maximum reactive power limit for each phase of dth ICs
$QT_d^{\min}, QT_d^{\max}$	minimum/maximum total reactive power limit for dth ICs
r	number of objective functions
R_j^k	resistance of the jth line
S^k	complex power of kth phase at the PCC
$\bar{S}$	average complex power at the PCC
$\tilde{S}$	average of the absolute power at the PCC
V_i^k	voltage of kth phase of ith bus
$V_i^{\min}, V_i^{\max}$	minimum/maximum voltage magnitude at ith bus
V_{ref}	reference voltage
VIF_i	voltage imbalance factor at ith bus
VDI_c	voltage deviation index for cth case study
$\text{VDI}^{\max}$	maximum VDI among all case studies
$\tilde{V}_c$	normalised VDI_C
w_i	weighting factors for the ith objective optimisation
X	set of decision variables
$\boldsymbol{Y}_{ih}^{km}$	admittance matrix element between kth phase of ith bus and mth phase of hth bus in the system
$\boldsymbol{Y}_{ih}^{abc}$	admittance matrix between ith and hth buses

Other symbols are defined in the text as they appear.

1 Introduction

Owing to the high penetration of distributed energy storage systems, renewable energy resources and different types of DC loads in microgrids, there are AC and DC buses in microgrids which form hybrid AC–DC microgrids [1]. This type of microgrid has been studied in literature from different points of view such as power flow algorithms, optimal dispatch, and control issues [2–6].

In hybrid AC–DC microgrids, the connection of AC and DC systems is possible through interlinking converters (ICs), therefore, several control schemes have been proposed for these ICs aiming at optimal DC load sharing between ICs or improving voltage quality as described in [7, 8], respectively. However, in most cases, due to unbalanced load conditions in the AC system, the microgrid is operated in unbalanced conditions [9]. Generally, there are two types of hybrid AC–DC microgrids; the first one includes one single DC bus connecting all DC loads and generations where this bus is linked to the AC system by one or several ICs. The second type is the situation where there are several separate DC buses in the system that each one is connected to the AC system by its own IC. In both types of hybrid AC–DC microgrids, unbalanced three-

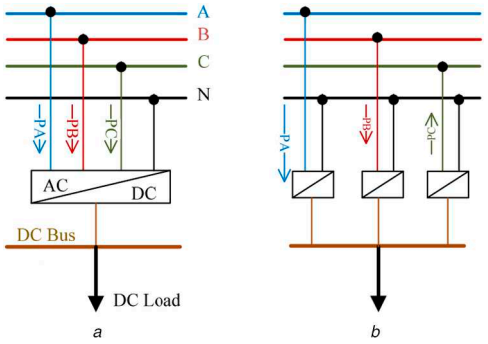

Fig. 1 *Control models of three-phase AC/DC converters*
(a) Symmetric model, ***(b)*** Asymmetric model

phase loading conditions would make major problems for optimal operation of the microgrid.

In the literature, several studies have focused on these issues especially in the islanded operating mode of microgrids. For example, in [9], a dynamic power routing strategy has been proposed for islanded operating mode of a type one unbalanced hybrid AC–DC microgrids to maximise the loadability at the distributed generations (DGs') buses. The proposed supervisory controller utilises an optimal power flow algorithm to minimise the microgrid load shedding in islanded operating mode. Numerical results verified the success of this method for maximising the loadability at generation buses. However, the second type of hybrid microgrids, with several independent DC buses, and microgrids in grid-connected mode have not been studied in this reference.

The voltage profile enhancement along with load sharing among DGs through a supervisory control scheme has been studied in [10, 11]. As proposed and verified in [10], compensation of unbalanced voltage and harmonics in the system is possible through a hierarchical control scheme using multiple current loop damping strategies in islanded microgrids. In [11], a novel control scheme is proposed for islanded microgrids with several dispatchable DGs to improve the performance of the microgrid by effectively compensating the negative-sequence currents of the unbalanced loads. However, none of the mentioned references consider the operation of the unbalanced microgrid in its grid-connected mode, where the droop control could not be implemented for sharing power among ICs. In [12], droop-controlled ICs are used to extend the autonomous power-sharing among DGs in both AC and DC systems and manage the power flow among different AC and DC resources. However, the optimal operation of this system under unbalanced load condition has not been investigated in this research. The coordination between DGs operation in both islanded and grid-connected modes of microgrid operation have been proposed in [13] where a complementary microgrid central controller is used to deploy secondary and tertiary control layers for DGs. This method is aimed to achieve seamless transitions between two operating modes using the cooperation of voltage and current and voltage controlled voltage sources inverters.

In [14], the voltage unbalance has been compensated in an islanded microgrid using a virtual output impedance method by measuring the negative-sequence voltage and current of DERs to find the voltage reference and tune the constant gain of closed-loop control. In [15], a robust control strategy for a grid-connected microgrid under unbalanced load condition was introduced using an adaptive Lyapunov control mechanism to mitigate the negative-sequence current due to unbalanced load conditions. A control scheme for unbalanced grid-connected microgrids was proposed in [16], which is based on the correction strategy to guarantee the voltage balance at the point of common coupling (PCC) by compensating the negative-sequence loads' currents.

In [17], the authors have proposed a supervisory control scheme for ICs aiming at increasing the microgrid's loadability at the PCC in grid-connected mode. The proposed method sets the active and reactive power bias factors for all three-phase ICs in such a way that keeps the power balance at the PCC. However, it does not optimise the system for this power balancing and just devotes the power imbalances to different phases of the ICs based on their capacities. Besides keeping the power balance at the PCC, numerical results in this reference demonstrate that the voltage deviations (VDs) at different busses are improved and grid losses are decreased due to keeping the power balance at the PCC. In [18], a two-step hierarchical power routing scheme for ICs in unbalanced hybrid AC–DC microgrids was proposed; in the first step, the optimisation tries to find an optimal power routing (OPR) within ICs to minimise the power losses in the system. At the second step, the proposed algorithm in [17] is used to keep the power balance at the PCC. However, the proposed hierarchical structure minimises the objective functions (OFs) sequentially not using a multi-objective optimisation algorithm.

To enhance the existing techniques for the optimal operation of unbalanced hybrid AC–DC microgrids in the grid-connected operating mode, in this paper a multi-objective optimisation model is proposed to minimise the PIF at the PCC, active power losses, and VD indices in a microgrid considering all operational constraints. In this model, the power routing is not only between three phases of each three-phase ICs, but also it is between different ICs in the microgrid. It means that the proposed scheme considers the load shifting between ICs during the optimisation process.

For this purpose, the rest of this paper is organised as follows. In Section 2, the single-phase control model for three-phase ICs is presented. The proposed OPR algorithm is described in Section 3. Section 4 is devoted to defining case studies and numerical results. Finally, the conclusions are presented in Section 5.

2 Control models of interlinking converters

Usually, a three-phase IC is operated as asymmetric converter where all three-phase loadings are the same and the same switching pattern is deployed for three phases considering phase shifting between three phases. However, it is possible to operate a converter unsymmetrically. It means that different phases could have different loading indices due to the system requirements. For the asymmetric operation of three-phase converters, we should replace them with four-lag converters in four-wire AC systems or we can use three-phase three-lag converters when Δ/Y transformers are implemented [9]. Therefore, we can model a three-phase converter as three single-phase converters as shown in Fig. 1. In both symmetric and asymmetric control models, we can use different techniques for active and reactive power of the converter including PQ control, droop control, and V/F control method. Since we are studying a grid-connected microgrid, we consider the PQ control strategy for our ICs [19].

Using this control method, the switching activates within the converter is controlled in such a way that the converter output satisfies active and reactive power according to its assigned *PQ* references as shown by (1) and (2).

$$P_d^k = P_d^{\mathrm{ref},k} \tag{1}$$

$$Q_d^k = Q_d^{\mathrm{ref},k} \tag{2}$$

Therefore, optimal tuning of *PQ* references will result in optimal operation of hybrid AC–DC microgrids as we will describe in the next sections. It should be mentioned that other control techniques like droop or V/F control methods are more appropriate for islanding operation mode of microgrids.

3 Proposed OPR scheme

The flowchart of the proposed OPR method is shown in Fig. 2 for *i*th operation interval. As it can be seen in this figure, the flowchart contains an optimisation algorithm which uses the system model and unbalanced power flow calculations during the optimisation process to optimise the operation of the system by routing the power between and within ICs.

The flowchart starts with updating the system model for the *i*th operating interval. It means that all forecasted renewable generations, load estimation and electric vehicles (EVs) charging

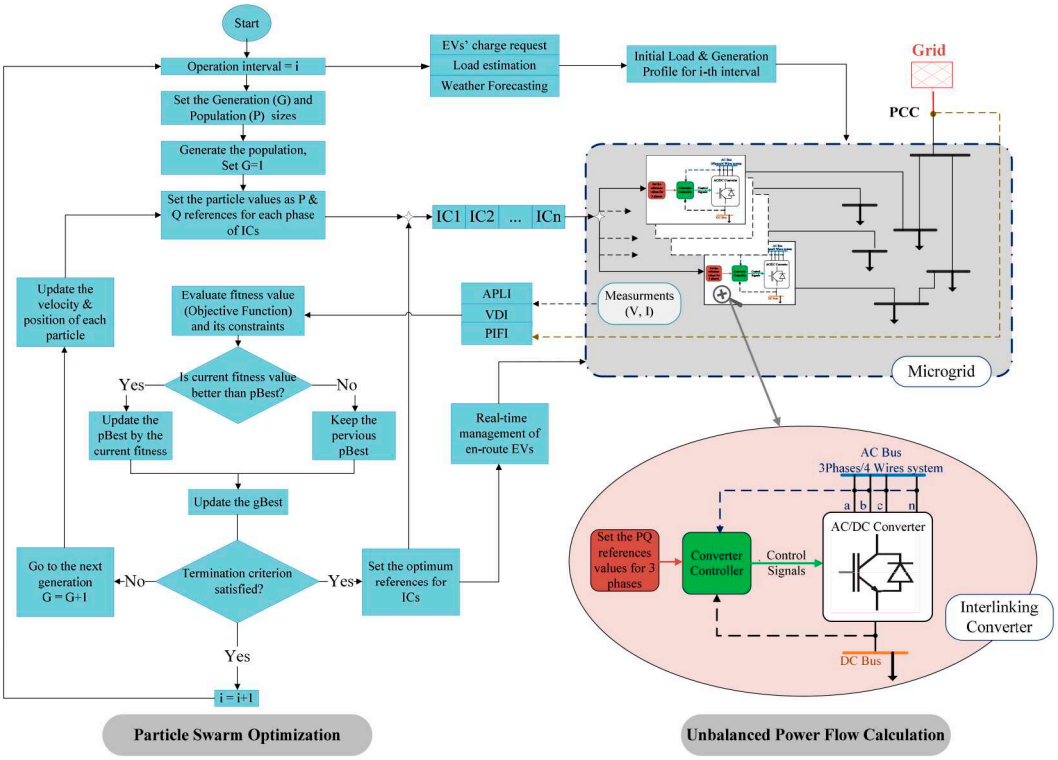

Fig. 2 *Proposed OPR scheme*

requests are collected to modify the microgrid model for the upcoming operating interval. Afterward, a modified PSO algorithm tries to solve a multi-objective optimisation model aiming at minimising the power imbalance factor (PIF) at the PCC, active power losses and VD index. The output of this optimisation is optimum *PQ* references for each phase of ICs in the system.

The ICs in this system are used by charging stations (CSs) to charge EVs. Therefore, to meet the optimisation output, an effective EV re-routing mechanism is required. As it can be seen in the flowchart, after PSO convergence, the output is sent to an agent for real-time management of en-route EVs. In [20], authors have proposed a cognitive price-based strategy for real-time management of en-route EVs which can motivate the EVs' owners to go to determined CSs based on the system requirement. Since this topic is out of the scope of this paper, here in this work we assume that optimal load sharing between ICs is doable using an effective re-routing mechanism as described in [20].

3.1 Multi-objective optimisation model

As mentioned before, in this problem there are three OFs to be optimised simultaneously. Therefore, a multi-objective optimisation model is needed. A multi-objective optimisation model is used for an optimisation problem with several OFs which may contradict each other. For this kind of optimisation problems, the concept of Pareto optimality can help to find an optimum solution for the problem. If this solution exists, it provides an efficient solution which means that it cannot be improved for one any of the OFs without having a negative effect on other OFs [21]. Generally, a multi-objective optimisation model can be written as follows:

$$\begin{aligned} &\min \ F(X) = (f_1(X),\ f_2(X), \ldots, f_r(X)) \\ &\text{Subject to: } AX \le B \end{aligned} \tag{3}$$

There are several solution methods for this problem such as the weighted-sum method, game-theoretical techniques etc. Between all these methods, the most common method is the weighted-sum method [22], where it uses weighting factors (w_i) to combine all OFs as a single OF shown by the following equation:

$$\begin{aligned} &\min \ F(X) = w_1 f_1(X) + w_2 f_2(X) + \cdots + w_r f_r(X) \\ &\text{Subject to: } AX \le B \end{aligned} \tag{4}$$

Choosing appropriate weighting factors for OFs is one of the most important issues in this method. These factors are selected based on the importance of each OF and usually, the trial and error method is deployed in this regard.

In this paper, three OFs are defined for the optimisation problem and the weighted-sum method is used to solve the problem. The OFs are defined as below:

1. $f_1(X)$ = Active power losses index (APLI)

This index is defined as total active power losses by transmission lines within the microgrid and is calculated by the following equation:

$$\text{APLI} = \sum_{j=1}^{L} \sum_{k} R_j^k \left| I_j^k \right|^2 \tag{5}$$

2. $f_2(X)$ = VD index (VDI)

The VD index is defined by (6).

$$\text{VDI} = \sum_{i=1}^{N} (\text{VDI}_i)^2 \tag{6}$$

where the VD index at *i*th bus of the system (VDI_i) is defined by (7) as the maximum value of VD from the reference voltage magnitude (e.g. 1 pu), between three phases.

$$\text{VDI}_i = \left(\left| V_i^k \right| - \left| V_{\text{ref}} \right| \right)^{\max} \tag{7}$$

3. $f_3(X)$ = Power imbalance factor index (PIFI)

To keep the power balance at the PCC, the PIF should be minimised at this point, therefore, the PIFI is defined by (8) which shows the maximum deviation of complex power between three phases from their average value.

$$\text{PIFI} = \left(\frac{1}{\bar{S}} \right) \times \max \left| S^k - \bar{S} \right| \tag{8}$$

where

$$\widehat{S} = (1/3) \cdot \sum_k S^k \tag{9}$$

$$\bar{S} = (1/3) \cdot \sum_k \left|S^k\right| \tag{10}$$

Hence, using the weighted-sum method and defining the problem constraints, the OF for this problem along with all constraints are presented by (11)–(19).

$$\min \text{OF} = w_1 \times \text{APLI} + w_2 \times \text{VDI} + w_3 \times \text{PIFI} \tag{11}$$

Subject to:

$$P_i^k + \text{j}Q_i^k = V_i^k \sum_{h=1}^{N} \sum_m \left(Y_{ih}^{km}\right)^* \left(V_h^m\right)^* \tag{12}$$

$$\sum_{d=1}^{D} \left(\sum_k P_d^k \right) = \sum_{d=1}^{D} \text{PT}_d \tag{13}$$

$$PT_d^{\min} \le \left(\sum_k P_d^k \right) \le PT_d^{\max} \tag{14}$$

$$QT_d^{\min} \le \left(\sum_k Q_d^k \right) \le QT_d^{\max} \tag{15}$$

$$P_d^{\min} \le P_d^k \le P_d^{\max} \tag{16}$$

$$Q_d^{\min} \le Q_d^k \le Q_d^{\max} \tag{17}$$

$$V_i^{\min} \le \left|V_i^k\right| \le V_i^{\max} \tag{18}$$

$$I_j^k \le I_j^{\max} \tag{19}$$

Equation (12) shows the unbalanced power flow equations as described in [23], where the admittance matrix of the microgrid is obtained by (18).

$$\mathbf{Y}_{ih}^{abc} = \begin{bmatrix} Y_{ih}^{aa} & Y_{ih}^{ab} & Y_{ih}^{ac} \\ Y_{ih}^{ba} & Y_{ih}^{bb} & Y_{ih}^{bc} \\ Y_{ih}^{ca} & Y_{ih}^{cb} & Y_{ih}^{cc} \end{bmatrix} \tag{20}$$

The load balance constraint is presented by (13) to make sure that the total load before and after the power routing is the same while the load could be transferred between ICs and also within three phases of each IC. The maximum and minimum capacity limits for active and reactive power of ICs are determined by (14) and (15), respectively. In addition, the active and reactive power limits for each phase of ICs, are reported by (16) and (17). Finally, the voltage magnitudes of each bus and feeders' currents should not exceed their pre-defined limits as shown by (18) and (19). By calculating the final active and reactive power values for each phase of the three-phase ICs, the *PQ* references are updated and set as below

$$P_d^{\text{ref},k} = P_d^{\text{opt},k} \tag{21}$$

$$Q_d^{\text{ref},k} = Q_d^{\text{opt},k} \tag{22}$$

Assuming that the re-routing mechanism is successful to manage mobile loads, these reference values are sent to ICs' controllers for tuning their active and reactive power outputs.

3.2 Particle swarm optimisation (PSO)

Generally, PSO is a proper optimisation algorithm for power system studies especially when non-linear power flow equations are included in the optimisation problem [24]. The PSO can also be implemented for solving multi-objective optimisation problems in power systems [25], however, other optimisation algorithms such as MOGA, NSGA, Taube search algorithms etc. could also be deployed for this purpose. In this paper, because of using the weighted-sum method, the multi-objective optimisation model is actually converted to a single-objective optimisation problem, therefore, the modified PSO algorithm can be considered as a good choice for this optimisation problem because it is strong enough to converge to an optimal solution over an acceptable solution time.

The modified PSO algorithm in this research is equipped with band coefficients and variables' direction control mechanisms which accelerate the PSO to move toward the optimal point while it does not lose the first feasible solution for the problem. The detailed description of this modification was presented in [26]. Fig. 2 demonstrates the steps in the PSO algorithm in details. As can be seen in this flowchart, the optimisation process is started by generating the first population of the PSO and selecting variables' values. Afterward, these values are set in the network model and unbalanced power flow is executed to obtain the results which are used to evaluate the OF. In each iteration, the global best is updated based on the best solution of that generation. Considering the best existing solution, variables' speeds are determined and the new generation of particles are created and this process continues until one of the optimisation criteria are reached. The output of PSO contains the optimum *PQ* references for each phase of ICs. The challenging issue for PSO algorithm is to find appropriate generation and population sizes which are different for each application. In this study, we determine these values for each system using the trial and error method. By finding the optimum solution of OPR, the load management between ICs is doable by the real-time rerouting mechanism.

3.3 Microgrid operating index (MOI)

Since the proposed OPR scheme includes a multi-objective optimisation which tries to minimise several indices, and also to compare the results of this method to the base study case and other case studies with algorithms that just focus on some of the indices, we can define the microgrid operating index (MOI) and its normalised value $\left(\tilde{M}_c\right)$ as an indicator that reflects the microgrid operating features as shown by (23) and (24).

$$\tilde{M}_c = \text{MOI}_c / \text{MOI}^{\max} \tag{23}$$

$$\text{MOI}_c = \left(\tilde{A}_c + \tilde{V}_c + \tilde{P}_c\right) \tag{24}$$

where in these equations

$$\tilde{A}_c = \text{APLI}_c / \text{APLI}^{\max} \tag{25}$$

$$\tilde{V}_c = \text{VDI}_c / \text{VDI}^{\max} \tag{26}$$

$$\tilde{P}_c = \text{PIFI}_c / \text{PIFI}^{\max} \tag{27}$$

Using this index, it is possible to compare different case studies with different OFs. From this definition, it is obviously clear that lower $\tilde{M}_c$ for a case study shows the better performance of the microgrid regarding the active power losses, VDs and PIF at the PCC.

4 Numerical results

To compare the results of the proposed method by other methods described in [17, 18], four case studies are defined in Table 1. As it can be seen in this table, C1 to C4 stands for case studies 1 to 4, respectively. C1 is the base case without any control and optimisation algorithm. In case two (C2), only the power routing

Table 1 Power routing mechanism and OFs for case studies

Study Case	Power Routing Mechanism		Objectives (Minimising)		
	Within ICs	Between ICs	PIFI	APLI	VDI
C1- Base Case	✗	✗	✗	✗	✗
C2- [17]	✓	✗	✓	✗	✗
C3- [18]	✓	✗	✓	✓	✗
C4- Proposed OPR	✓	✓	✓	✓	✓

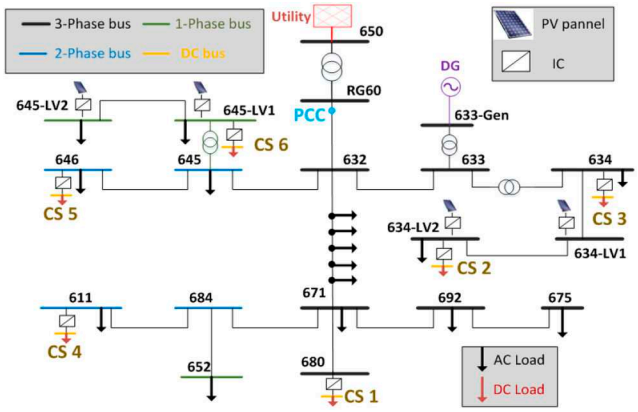

Fig. 3 *Unbalance hybrid AC–DC microgrid [17]*

Table 2 Loads data at 8 PM

Terminal	Power factor	Phase_*A*, kW	Phase_*B*, kW	Phase_*C*, kW
680	0.97	33.3	271.7	39.3
634-LV2	0.95	46.9	26.1	13.2
634	0.98	59.4	112.2	112.2
611	0.95	0.0	0.0	64.8
646	0.40	0.0	76.2	0.0
645-LV-1	0.44	6.6	0.0	0.0
DL1	0.87	1.9	7.4	13.1
DL2	0.87	0.2	0.7	1.3
DL3	0.87	2.4	9.2	16.3
DL4	0.87	1.7	6.6	11.7
DL5	0.87	0.6	2.4	4.2
671	0.87	215.4	215.4	215.4
611	0.90	0.0	0.0	91.2
634-LV2	0.81	40.5	29.4	30.0
634	0.81	79.7	59.8	59.8
645-LV-1	0.81	42.4	0.0	0.0
645-LV-2	0.81	0.0	46.1	0.0
646	0.87	0.0	75.8	36.9
652	0.83	66.4	0.0	0.0
675	0.88	241.7	33.9	144.5
692	0.75	0.0	0.0	63.1
680	0.97	33.3	271.7	39.3

mechanism is deployed to remove the unbalances at the PCC using a supervisory control scheme as described in [17]. This method tries to devote the unbalancing value at the PCC to the ICs regarding their capacities C3 is reflecting the results from the proposed method in [18] which minimises the active power losses and PIF at the PCC hierarchically. And finally, C4, which is the proposed OPR method in this paper, uses the power routing between and within ICs to minimise the active power losses, PIF at the PCC and the voltage deviation index for all buses within the microgrid.

All these case studies will be analysed through numerical results by implementing these methods on the modified IEEE 13-bus system as a highly unbalanced hybrid AC–DC microgrid. Furthermore, to prove the capabilities of the proposed OPR scheme in distribution systems, this method is also examined on the IEEE 34-bus system as an unbalanced distribution network. Finally, Florida International University (FIU) smart grid testbed is studied to show the effect of OPR between ICs in losses reduction in an actual smart microgrid.

4.1 Modified IEEE 13-bus system

The modified IEEE 13-bus system is shown in Fig. 3. In [17], the details of modifications have been reported and Tables 2–5 contain data of this system. In this microgrid, CS1, CS2, and CS3 are CSs with three-phase interlinking converters (IC#1, IC#2 and IC#3) while CS4, CS5 and CS6 indicate CSs containing single-phase ICs. In this paper, the system is modelled in DigSilent PowerFactory2019, as a professional power system software [27, 28], and the DigSilent Programming Language is used to develop all algorithms related to the four case studies. Figs. 4 and 5 demonstrate the active power losses and PIF of the system during a

Table 3 Transformers data

Terminal *i*	Terminal *j*	HV, KV	LV, KV	Short-Circuit voltage, %
substation HV	650	115	4.16	8.06
645	645-LV-1	2.4	0.24	3
633-Gen	633	6.6	4.16	6
633	634	4.16	0.48	2.28

Table 4 Generation data at 8 PM

	Terminal	Controller	Active Power, KW	Reactive Power, Kvar	Voltage, p.u
ext. Grid	650	Swing	1789.94	1170.09	1.00
DG	633-Gen	*P-V*	839.25	406.47	1.04
PV 634–1	634-LV1	*P-Q*	75.77	0.00	—
PV 634–2	634-LV2	*P-Q*	49.32	0.00	—
PV 645–1	645-LV1	P-Q	13.96	0.00	—
PV 645–2	645-LV2	*P-Q*	25.98	0.00	—

Table 5 Lines data

From	to	Length, ft	Rate, KA	R1, Ω	X1, Ω
634	634-LV1	200	0.68	0.0050	0.0021
634-LV1	634-LV2	300	0.68	0.0075	0.0032
684	652	800	0.165	0.2220	0.0795
692	675	500	0.26	0.0340	0.0420
632	633	500	0.68	0.0569	0.0719
632	645	500	0.92	0.1068	0.0845
632	671	2000	1.46	0.0117	0.0364
645	646	300	0.92	0.0641	0.0507
645-LV-1	645-LV-2	100	0.40	0.0030	0.0030
RG60	632	2000	1.46	0.0704	0.2187
671	680	1000	1.46	0.0352	0.1093
671	684	300	0.92	0.0641	0.0507
684	611	300	0.92	0.0694	0.0921
671	692	10	0.26	0.0007	0.0008

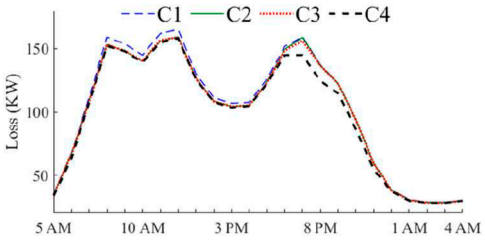

Fig. 4 *Losses for four cases for 24 h*

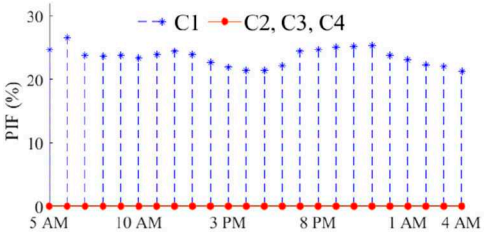

Fig. 5 *PIF at the PCC for 24 h*

24-hour operation interval for C1 to C4. As can be seen in Fig. 4, maximum and minimum active power losses are reported for C1 and C4, respectively. Fig. 5 shows that in C2, C3, and C4, the PIF at the PCC is zero while in C1, the PIF is fluctuating between 23 to 27%. It is because of this fact that the OFs in C2, C3, and C4 are aimed to minimise the PIF at the PCC.

To compare the voltage profiles in all case studies, in addition to VDI which is used in the optimisation model, we can calculate the voltage imbalance factor (VIF) by (28) for each bus of the system to measure the unbalances between three phases in unbalanced microgrids [29].

$$\mathrm{VIF}_i = \frac{\left(\left|V_i^k\right| - \mathrm{Ave}\left|V_i^k\right|\right)^{\max}}{\mathrm{Ave}\left|V_i^k\right|} \times 100 \tag{28}$$

Fig. 6 shows the VIFs at bus 671 of the system for all case studies. It can be seen that the VIF is fluctuating between 2 to 8% in C1 while it is <2% in C2, C3, and C4 over this 24-hour operating interval. It means that in all proposed methods in C2, C3, and C4 the voltage profile of the system buses is improved. This fact will be reported in detail when system indices are calculated.

To validate the results from each case study, here we focus on the results for one operating interval and finally we will calculate the system indices to compare the results from four case studies. The numerical results are reported for 8 PM in details by Figs. 7–13. Since the main goal in this study is to keep the power balance at the PCC and to achieve this goal in C4 (the proposed OPR optimisation model), we need to consider a high weighting factor for PIFI as shown the following equation:

$$w_3 >> w_2, w_1 \tag{29}$$

In this study, and as shown in Fig. 8, the initial values for, PIFI, VDI, and APLI are around 25, 18, and 160, respectively. In this case, and to dominate the impact of PIFI on the final OF value, at first we set $w_3 = 30$ (the weighting factor for PIFI) while we adjusted $w_2 = w_1 = 1$. Afterward, and by running the optimisation, we observed that the PSO just minimises the PIFI and its effect on the other indexes is negligible. So we gradually decreased w_3 from 30 step by step, and run the optimisation receptively. Finally our

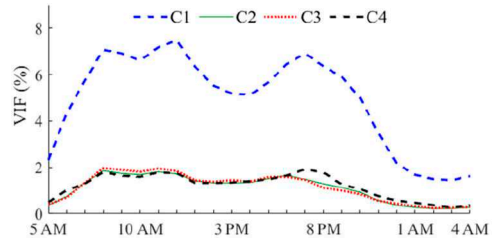

Fig. 6 *VIF at bus 671 for 24 h*

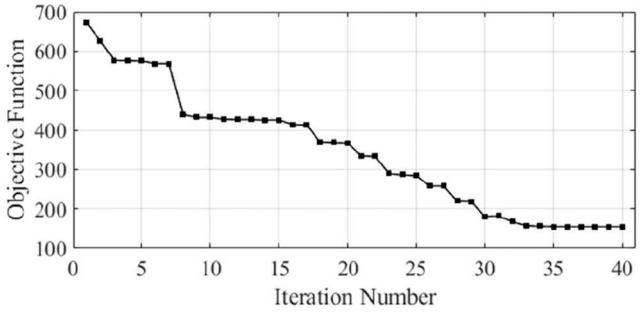

Fig. 7 *OF values for each iteration of PSO*

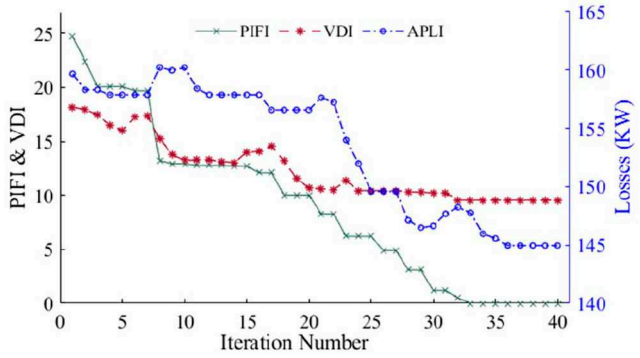

Fig. 8 *Values of PIF, VDI, and APLI for each iteration of PSO*

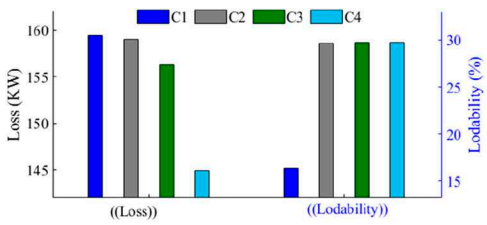

Fig. 9 *Microgrid active power losses and loadability*

simulation results demonstrated that if the $w_3 = 20$, by choosing $w_2 = w_1 = 1$, the final OF could satisfy our expectations for minimising the PFIF as well as reducing the VDI and active power losses.

In this study, a core i7 CPU 3.40 GHz with 8 GB of memory (RAM) computer is used for system simulation and running the optimisation program. For the modified 13-bus system, we define the population size and maximum generation size of the PSO by 150 and 40, respectively. We also determined these values using the trial and error method. However, the difference is that at the first, we selected very high values for both the population size and maximum generation size by 400 and 250, respectively, and run the PSO several times. The reason was to find an optimum solution without considering the solution time (in this case the computational time was around 197 s). Since decreasing the population size and maximum generation size significantly reduce the computational time, we set a 3% error for final solution while we could decrease the solution time from 197 s (for the population size and maximum generation size of 400 and 250, respectively) to 38.6 s for population size and maximum generation size of the PSO by 150 and 40, respectively.

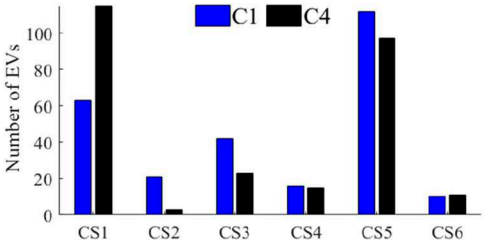

Fig. 10 *EVs distribution*

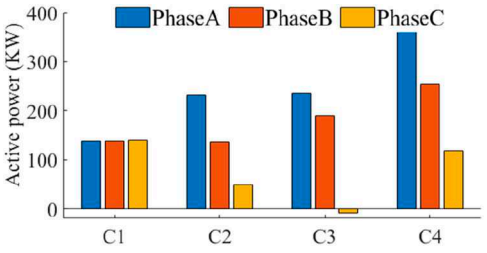

Fig. 11 *Active power of IC#1*

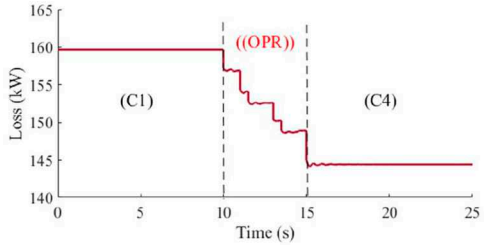

Fig. 12 *Microgrid losses for C1 and C4*

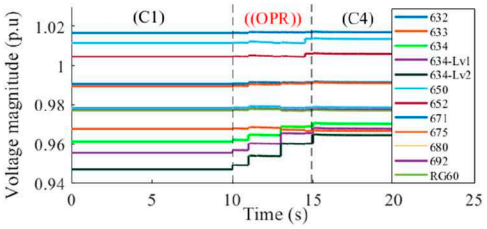

Fig. 13 *Voltage profiles for C1 and C4*

Numerical results show the algorithm is fast enough for this application which tries to optimise the system for the next operating interval. Fig. 7 shows the value of the OF during the optimisation and Fig. 8 demonstrates the values of PIFI, VDI, and APLI in this optimisation process. As it can be observed from these two figures, minimising the PIFI is dominant to VDI and APLI and it finally goes to zero at the 33rd iteration of the PSO. The general trend of APLI and VDI shows that they are also decreasing but they have some fluctuations before reaching their final optimum values.

Fig. 9 shows the microgrid active power losses and loadability for all case studies. As it can be seen in this figure, proposed OPR scheme (C4) will result in the least active power losses and the same loadability index comparing with C2 and C3. The distribution of mobile loads for the first three case studies would be the same as shown by Fig. 10 because in these cases we do not shift the loads between ICs while in C4, the proposed OPR model optimises the distribution of EVs between ICs. It can be seen that the number of EVs for CS1 is increased significantly while it is decreased for CS2, CS3, and SC5. CS4 and CS6 do not experience huge differences. Fig. 11 represents the active power for each phase of IC#1 as an example of three-phase ICs in the system. It is obviously clear that except in C1, in other case studies this IC is operated asymmetrically. It is because of this fact that the asymmetric operation of this converter results in minimum PIFI at the PCC (in this case PIFI is zero) and also improvement in the system indices.

Table 6 System indices at 8 PM

Study Case	$PIFI_c$	VDI_c	$APLI_c$	$\tilde{M}_c$
(C1)	24.43	0.0673	159.4452	1.0000
(C2)	0.00	0.0261	159.0393	0.4618
(C3)	0.00	0.0252	156.2815	0.4515
(C4)	0.00	0.0192	144.9713	0.3982

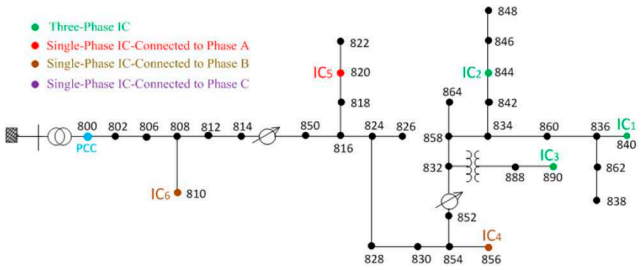

Fig. 14 *Modified IEEE 34-bus test system with six ICs*

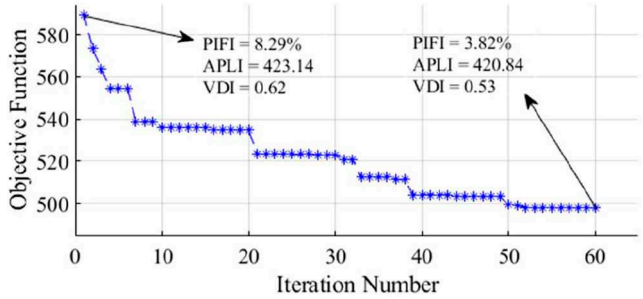

Fig. 15 *OF values for IEEE 34-bus system*

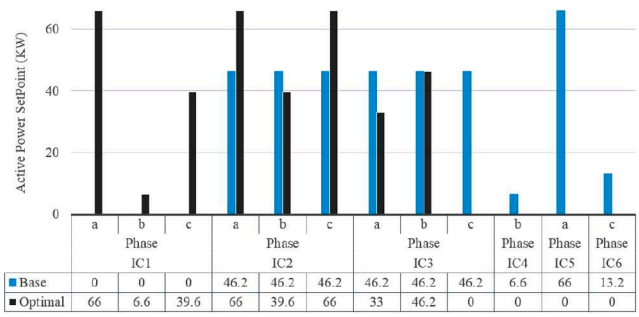

Fig. 16 *Reference active power for all phases of ICs for base and optimal scenarios*

In addition to static simulations for this 24-hour operating interval, quasi-dynamic simulations have been executed for this operation interval to show the dynamic performance of the system regarding the proposed OPR method in C4. Fig. 12 illustrates the active power losses and Fig. 13 shows the voltage profile of all AC buses in the system for the base case (C1) and the proposed optimum case (C4). We simulated the power routing schemes gradually to see the changes clearly.

As can be seen in this figure and also Fig. 9, the system loss is decreased from 159 kW in C1 to 144 kW in C4. From Fig. 13, it can be concluded that the optimum power routine scheme has improved the voltage profile significantly. For example, the voltage of bus 632-LV2 in C1 is <0.95 p.u. while it is in an acceptable range in C4. To evaluate the best performance of the system between these four case studies, we need to calculate the normalised value of MOI $(\tilde{M}_c)$ for all case studies as shown in Table 6. Since the lowest value reflects the better performance of the system, following we can classify all case studies.

$$\tilde{M}_{C4} < \tilde{M}_{C3} < \tilde{M}_{C2} < \tilde{M}_{C1} \tag{30}$$

This classification shows that C4, the proposed OPR method, has the minimum microgrid operating. The second rank of this classification is for C3, the hierarchical power routing scheme. C2, the supervisory control method, has the third rank and C1, system without any control and optimisation mechanism, has the biggest system operating index among these case studies. Although both supervisory control scheme and hierarchical power routing scheme are successful to improve the operation of unbalanced hybrid microgrids, the proposed multi-objective optimisation method leads to best results for optimal operation of hybrid microgrids.

4.2 IEEE 34-bus test system

The proposed OPR method in this paper can be also implemented in unbalanced distribution systems containing three-phase four-lag ICs. To validate the capabilities of the proposed OPR scheme in the distribution system, the IEEE 34-bus test system is selected as an example of unbalanced distribution system [30]. In this system, we need to locate some three-phase and single-phase ICs to the system. For this purpose, we replaced three balanced loads at buses 840, 844, and 890 with three-phase, four-lag AC/DC converters. Furthermore, the single-phase loads at buses 810, 820, and 856 also replaced by single-phase AC/DC converters. The single line diagram of the system along with all modification is shown in Fig. 14.

To optimise the system using the proposed OPR method, we set the population and generation sizes of the PSO as 150 and 60, respectively. Fig. 15 shows the values of OF from the first iteration to the last one.

The solution time for this case was 53.8 s which is still in the acceptable range for this problem. As shown in Fig. 15, the OPR scheme is successful to reduce PIFI from 8.29% in the first iteration to 3.82% in the last iteration. It is also decreasing the APLI and VDI from 423.14 KW and 0.62–420.84 and 0.53 p.u, respectively.

Fig. 16 indicates the results of the optimisation for the variables. It shows the active power set points for all phases of ICs in the system before (Base case) and after (Optimal) the optimisation. The results show that the optimisation is changing these values in their optimum direction to meet OF requirements.

4.3 FIU smart grid testbed

The FIU smart grid laboratory system has been established with required hardware and software for real-time operation of a small-scale power system. This system includes four synchronous generators along with four Synchro switches which make it possible to synchronise the generators together or with the utility. There are different types of DC and AC loads in this system. For example, there are four programmable AC loads which can vary from 0 to 3 kW. In this system, data acquisition systems are implemented to monitor all nodes and branches of the microgrid. The system data are available in [31]. This system is reconfigurable and based on the case study, we can change the configuration of the system. In this system, all measurements are collected remotely via a TCP/IP connection at the supervisory control and data acquisition SCADA) system which has been developed in LabVIEW, where it is possible to monitor and control all the system equipment, remotely. Fuses and intelligent electronic devices are used in this system for protection purposes. Fig. 17 shows the FIU smart grid test bed and Fig. 18 demonstrates the single-phase diagram of the 7-bus system which contains two synchronous generators and four programmable loads. We consider these loads as CSs and we want to show the effect of power routing between ICs on the system losses.

In this platform, a dynamic data exchange (DDE) is activated to transfer data between DIgSILENT PowerFactory (as the system simulator and optimisation software), and LabVIEW (as the SCADA system). Software interoperability in this study is shown in Fig. 19 where the optimisation process controls the SCADA through the DDE. Although system loads are voltage-dependent, approximately each load step is around 248 W and each load has ten steps. To run the optimisation, we consider that the charging rate of each EV is 248 W and therefore, each CSs can serve from 0

to 10 EVs. To get the numerical results, we run the system in two scenarios:

At the first scenario (Scenario 1), the total load of the system is increasing from 5520 to 7446 W. The active power set points for DG1 and DG2 are 1 and 1.5 kW, respectively. The distribution of EVs at the beginning of this period ($t = i$) is shown in Fig. 20. The loads gradually change in two steps to reach their final values at $t = i + 1$. S1 and S2 stand for step1 and step2 in Table 7.

In the second scenario (Scenario 2), the system is run from exactly the previous starting point but the same amount of load increase occurs in the system by the different distribution of EVs among ICs as shown in Fig. 21.

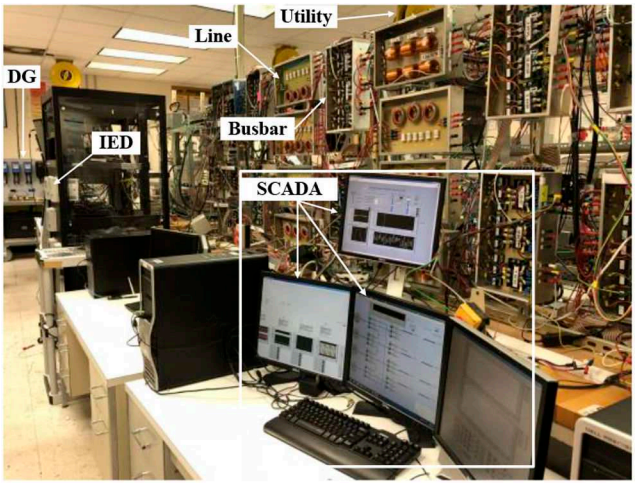

Fig. 17 *FIU smart grid testbed*

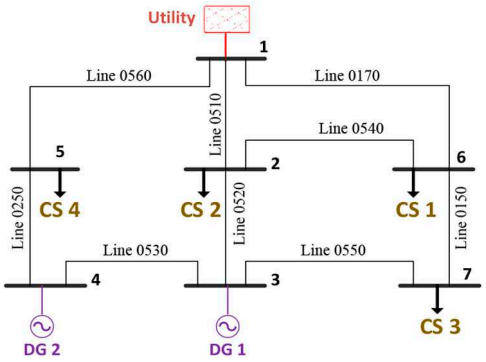

Fig. 18 *Single line diagram of the seven-bus test system at FIU*

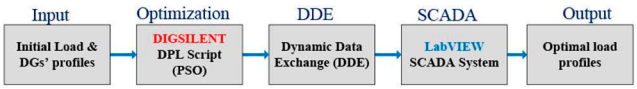

Fig. 19 *Software interoperability at FIU smart grid*

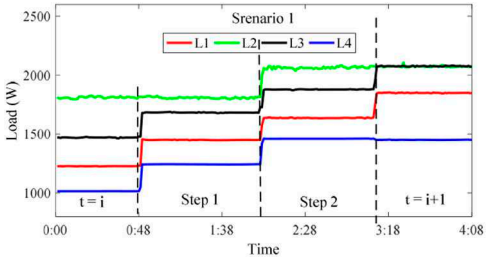

Fig. 20 *Load distribution in Scenario 1*

Table 7 EVs' distribution in Scenarios 1 and 2

CSs	Programmable loads distribution in Scenario 1				EVs distribution in Scenario 2			
	$t = i$	S1	S2	$t = i + 1$	$t = i$	S1	S2	$t = i + 1$
CS1	5	6	7	8	5	6	7	7
CS2	7	7	8	8	7	8	9	10
CS3	6	7	8	9	6	5	4	4
CS4	4	5	6	6	4	6	8	10
Sum	22	25	29	31	22	25	28	31

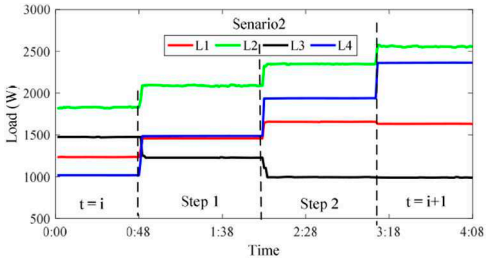

Fig. 21 *Load distribution in Scenario 2*

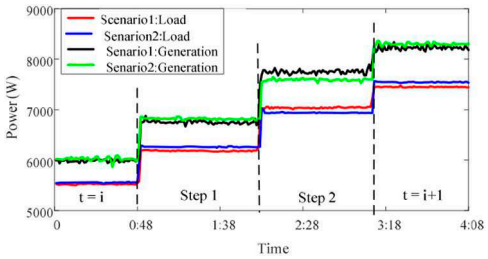

Fig. 22 *Total generation and load in both scenarios*

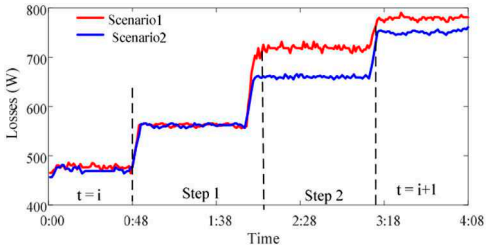

Fig. 23 *Active power losses in both scenarios*

The generation and load in both scenarios are shown in Fig. 22 and the differences between these values are indicated in Fig. 23 where the active power losses decrease from 789 W in Scenario 1 to 752 W in Scenario 2. The base distribution of EVs along with their distributions in the two steps of load variations in both scenarios is reported in Table 7. In both scenarios, the total number of EVs is increasing from 22 (at $t = i$) to 31 (at $t = i + 1$) while the EVs' distribution between CSs is different. The optimal distribution (Scenario 2) shows an increase in the number of EVs in CS2 and CS4 while it decreases the EVs from CS1 and CS3 comparing with Scenario 1. This redistribution leads to 4.67% of loss reduction in this system.

5 Conclusion

In this paper, an OPR scheme between and within ICs was proposed to minimise the PIF at the PCC, active power losses and VD indices in the grid-connected mode of an unbalanced hybrid AC–DC microgrid, where there are several independent ICs in the system. The effectiveness of the developed algorithm was confirmed through numerical results obtained from the simulation of the modified IEEE 13-bus system as a highly unbalanced hybrid AC–DC microgrid and IEEE 34-bus test system as an unbalanced distribution system. Furthermore, to show the effect of the power routing between CSs on the active power losses reduction, a laboratory-based smart microgrid was established and examined. Numerical results demonstrated that the proposed OPR scheme was highly successful to minimise the OFs and smooth the voltage profile within the system. Consequently, optimal operation of unbalanced hybrid AC–DC microgrids would be possible when the proposed OPR algorithm is implemented.

6 Acknowledgments

Part of this work was supported by grants from the US Department of Energy. The authors are with the Energy System Research Laboratory, ECE Department. Florida International University, Miami, FL, 33174 USA.

7 References

[1] Eghtedarpour, N., Farjah, E.: 'Power control and management in a hybrid AC/DC microgrid', *IEEE Trans. Smart Grid*, 2014, **5**, (3), pp. 1494–1505

[2] Nassar, M.E., Hamad, A.A., Salama, M.M., *et al.*: 'A novel load flow algorithm for islanded AC/DC hybrid microgrids', *IEEE Trans. Smart Grid*, 2017, **10**, pp. 1553–1566

[3] Hamad Amr, A., Azzouz, M.A., El Saadany, E.F.: 'A sequential power flow algorithm for islanded hybrid AC/DC microgrids', *IEEE Trans. Power Syst.*, 2016, **31**, (5), pp. 3961–3970

[4] Aprilia, E., Meng, K., Hosani, M.A., *et al.*: 'Unified power flow algorithm for standalone AC/DC hybrid microgrids', *IEEE Trans. Smart Grid*, 2017, **10**, pp. 639–649

[5] Zhao, B., Haifeng, Q., Qin, R., *et al.*: 'Robust optimal dispatch of AC/DC hybrid microgrids considering generation and load uncertainties and energy storage loss', *IEEE Trans. Power Syst.*, 2018, **33**, pp. 5945–5957

[6] Battistelli, C., Agalgoankar, Y.P., Pal, B.C.: 'Probabilistic dispatch of remote hybrid microgrids including battery storage and load management', *IEEE Trans. Smart Grid*, 2017, **8**, (3), pp. 1305–1317

[7] Lu, X., Guerrero, J.M., Sun, K., *et al.*: 'Hierarchical control of parallel AC-DC converter interfaces for hybrid microgrids', *IEEE Trans. Smart Grid*, 2014, **5**, (2), pp. 683–692

[8] Baharizadeh, M., Karshenas, H.R., Guerrero, J.M.: 'Control strategy of interlinking converters as the key segment of hybrid AC–DC microgrids', *IET Gener. Transm. Distrib.*, 2016, **10**, (7), pp. 1671–1681

[9] Allam, M.A., Hamad, A.A., Kazerani, M., *et al.*: 'A novel dynamic power routing scheme to maximize loadability of islanded hybrid AC/DC microgrids under unbalanced AC loading', *IEEE Trans. Smart Grid*, 2018, **9**, (6), pp. 5798–5809

[10] Han, Y., Shen, P., Zhao, X., *et al.*: 'An enhanced power sharing scheme for voltage unbalance and harmonics compensation in an islanded microgrid', *IEEE Trans. Energy Convers.*, 2016, **31**, (3), pp. 1037–1050

[11] Hamzeh, M., Karimi, H., Mokhtari, H.: 'A new control strategy for a multi-bus MV microgrid under unbalanced conditions', *IEEE Trans. Power Syst.*, 2012, **27**, (4), pp. 2225–2232

[12] Loh, P.C., Li, D., Chai, Y.K., *et al.*: 'Autonomous operation of hybrid microgrid with AC and DC subgrids', *IEEE Trans. Power Electron.*, 2013, **28**, (5), pp. 2214–2223

[13] Micallef, A., Apap, M., Spiteri-Staines, C., *et al.*: 'Single-phase microgrid with seamless transition capabilities between modes of operation', *IEEE Trans. Smart Grid*, 2015, **6**, (99), pp. 2736–2745

[14] Savaghebi, M., Jalilian, A., Vasquez, J.C., *et al.*: 'Autonomous voltage unbalance compensation in an islanded droop-controlled microgrid', *IEEE Trans. Ind. Electron.*, 2013, **60**, (4), pp. 1390–1402
[15] Rezaei, M.M., Soltani, J.: 'A robust control strategy for a grid-connected multi-bus microgrid under unbalanced load conditions', *Int. J. Electr. Power Energy Syst.*, 2015, **71**, pp. 68–76
[16] Shi, H., Zhuo, F., Yi, H., *et al.*: 'Control strategy for microgrid under three-phase unbalance condition', *J. Mod. Power Syst. Clean Energy*, 2016, **4**, (1), pp. 94–102
[17] Mahmoudian Esfahani, M., Mohammed, O.: 'Loadability improvement of unbalanced hybrid AC-DC microgrids using a supervisory control scheme for interlinking converters'. IEEE PES ISGT Asia, Singapore, 2018
[18] Esfahani, M.M., Habib, H.F., Mohammed, O.A.: 'A hierarchical power routing scheme for interlinking converters in unbalanced hybrid AC-DC microgrids'. IEEE IECON 2018, Washington DC, USA, 2018
[19] Carrasco, G., Silva, C.A., Peña, R., *et al.*: 'Control of a four-lag converter for the operation of a DFIG feeding stand-alone unbalanced loads', *IEEE Trans. Ind. Electron.*, 2015, **62**, (7), pp. 4630–4640
[20] Hariri, A., Mahmoudian Esfahani, M., Mohammed, O.: 'A cognitive price-based approach for real-time management of en-route electric vehicles'. 2018 IEEE Transportation Electrification Conf. and Expo (ITEC), Long Beach, CA, USA, 2018, pp. 922–927
[21] Konak, A., Coit, D.W., Smith, A.E.: 'Multi-objective optimization using genetic algorithms: a tutorial', *Reliab. Eng. Syst. Saf.*, 2006, **91**, (9), pp. 992–1007
[22] Kim, I.Y., de Weck, O.L.: 'Adaptive weighted-sum method for bi-objective optimization: Pareto front generation', *Struct. Multidiscip. Optim.*, 2005, **29**, (2), pp. 149–158
[23] Sereeter, B., Vuik, K., Witteveen, C.: 'Newton power flow methods for unbalanced three-phase distribution networks', *Energies*, 2017, **10**, (10), p. 1658
[24] Del Valle, Y., Venayagamoorthy, G.K., Mohagheghi, S., *et al.*: 'Particle swarm optimization: basic concepts, variants and applications in power systems', *IEEE Trans. Evol. Comput.*, 2008, **12**, (2), pp. 171–195
[25] Wang, L., Singh, C.: 'Environmental/economic power dispatch using a fuzzified multi-objective particle swarm optimization algorithm', *Electr. Power Syst. Res.*, 2007, **77**, (12), pp. 1654–1664
[26] Mahmoudian Esfahani, M., Sheikh, A., Mohammed, O.: 'Adaptive real-time congestion management in smart power systems using a real-time hybrid optimization algorithm', *Electr. Power Syst. Res.*, 2017, **150**, pp. 118–128
[27] Lammert, G., Ospina, L.D.P., Pourbeik, P., *et al.*: 'Implementation and validation of WECC generic photovoltaic system models in DIgSILENT PowerFactory'. 2016 IEEE Power and Energy Society General Meeting (PESGM), Boston, MA, USA, 2016, pp. 1–5
[28] Kim, I., Regassa, R., Harley, R.G.: 'The modeling of distribution feeders enhanced by distributed generation in DIgSILENT'. 2015 IEEE 42nd Photovoltaic Specialist Conf. (PVSC), New Orleans, LA, USA, 2015, pp. 1–5
[29] IEEE Std. 112–2004.: 'IEEE Standard Test Procedure for Polyphase Induction Motors and Generators'
[30] Kersting, W.H.: 'Radial distribution test feeders'. 2001 IEEE Power Engineering Society Winter Meeting. Conf. Proc. (Cat. No. 01CH37194), New York, NY, USA, 2001, vol. 2, pp. 908–912
[31] Salehi, V., Mohamed, A, Mazloomzadeh, A., *et al.*: 'Laboratory-based smart power system, part I: design and system development', *IEEE Trans. Smart Grid*, 2012, **3**, (3), pp. 1394–1404